Damage detection of composite beams via variational mode decomposition of shear slip data

Faraz Sadeghi[1,2], Mohsen Mousavi[3], Xinqun Zhu[4], Maria Rashidi[5], Bijan Samali[6], and Amir H. Gandomi[7,*]

[1]Research Fellow, Centre for Infrastructural Engineering, Western Sydney University, Penrith, NSW 2751, Australia, f.sadeghi@westernsydney.edu.au

[2]Structural Engineer, AECOM, Sydney, NSW 6000, Australia, f.sadeghi@westernsydney.edu.au

[3]Postdoctoral Research Associate, Faculty of Engineering & IT, University of Technology Sydney, Ultimo, NSW 2007, Australia, mohsen.mousavi@uts.edu.au

[4]Associate Professor, School of Civil and Environmental Engineering, University of Technology Sydney, Ultimo, NSW 2007, Australia, xinqun.zhu@uts.edu.au

[5]Senior Lecturer, Centre for Infrastructural Engineering, Western Sydney University, Penrith, NSW 2751, Australia, m.rashidi@westernsydney.edu.au

[6]Professor, Centre for Infrastructural Engineering, Western Sydney University, Penrith, NSW 2751, Australia, b.samali@westernsydney.edu.au

[7,*]Professor, Faculty of Engineering & IT, University of Technology Sydney, Ultimo, NSW 2007, Australia, gandomi@uts.edu.au

ABSTRACT

Damage of shear connectors in steel-concrete composite beams (SCC) affects the composite action and appears as abnormalities in the shear slip between the composite components. The shear slip at the composite interface causes nonlinearity in the global composite beam response which is an issue beyond the inherent complexity of the composite system. This paper presents a novel approach for damage detection of SCCs by variational mode decomposition (VMD) of shear slip data. Numerical and experimental studies were conducted on steel-concrete composite beams to generate noise-contaminated shear slip data from undamaged and damaged states of the structure. The VMD algorithm is employed to decompose shear slip signals into Intrinsic Mode Functions (IMFs) and then, the centre frequency of each mode is captured. The higher centre frequency realised in the second mode is taken as a damage sensitive feature. Since IMFs curves are extracted from the signal splines interpolated between the average of the peaks and troughs, the change of energy in the centre frequencies of the undamaged and damaged states can be defined as a damage index. Welch power spectral densities of the IMFs are calculated to further investigate changes in the centre frequencies of IMFs obtained using the VMD algorithm. The empirical mode decomposition (EMD) technique is also utilised to decompose shear slip signals into IMFs for comparison purposes while the mode-evaluation criteria for an IMF are somewhat different between the VMD and EMD. The results show that the EMD is not able to detect abnormalities in the shear slip signals affected by damage because of losing information through several mode decompositions and a phenomenon termed mode mixing. However, when the VMD was set to decompose the signal into two more successful in maintaining the frequency content of the shear slip signal. According to the results, the proposed method has been proved successful in detecting damage of composite beams and can be employed as a reliable and robust technique.

Keywords: Steel-concrete composite beams, Damage detection, Signal processing, Variational mode decomposition, Shear slip

INTRODUCTION

Structural health monitoring (SHM) is defined as employing sensing techniques and structural characteristics analysis to assess structural conditions and degradation. To ensure the safety and reliability of civil infrastructures such as bridges, innovative SHM methods have been developed by integrating advanced data analysis techniques. Damage detection methods consider bridges in terms of the basic structural systems such as beam, truss, cable-stayed and suspension. For the beam bridges whose decks are steel-concrete composite beams, different methods based on dynamic and static measurements are described in the literature (An et al. 2019).

Composite flooring systems such as steel-concrete composite (SCC) beams have been widely used in beam bridges, and this trend will continue to increase as they have desirable characteristics, such as being lightweight, having high stiffness, and possessing great strength (Nguyen et al. 2011; Sadeghi et al. 2020; Sadeghi 2021). The operational life of an SCC beam depends on its shear connection health. Besides, the severity of external loads is a crucial factor in SCC beam behaviour (Chen et al. 2019a). If the applied load exceeds its load-bearing capacity, massive displacements will take place that could lead to failure, visible damage and open cracks.

If the friction force at the interface of an SCC beam is overcome by an external load, its bond strength may fail, which reduces its overall rigidity and ultimate strength (Dilena and Morassi 2004). The bond strength failure causes the composite layers to have vertical uplift, tear, and/or shear slip. The shear slip, which is an inherent relative displacement between the composite layers, causes the concrete slab and steel girder to respond independently to loading and significantly affects the SCC beam load-bearing capacity and performance (Li et al. 2013; Li and Hao 2016).

Damage detection of beam bridges can be studied in terms of two types of damage. The first is the local stiffness reduction (e.g. open cracks or shear connection looseness) which is generally modelled by a massless rotational spring. The second is the reduced stiffness in an extensive area of the beam caused by fatigue damage. The latter type of damage that occurs due to fatigue, corrosion, or overstressing is a further reason for failure in the bond strength causing excessive interface shear slip and loss in the composite action (Vasdravellis and Uy 2014; Ho et al. 2015; Li et al. 2015). Research by Nie and Cai (Nie and Cai 2003) showed that damage to the shear connectors causes extra shear slip between concrete and steel, resulting in a stiffness degradation of 17% in the SCC bridge decks. Zhang et al. (Zhang et al. 2019) developed a mechanical model to predict shear slip and deflection in steel-concrete composite beams. They used a non-linear spring to model the composite shear connection and showed that neglecting shear slip can result in an error in deflection measurement up to 35%.

The interface damage identification of the SCC beams is not easy as the shear slip depends on the load and results in nonlinearity in the composite beam behaviour. Besides, direct inspection is impossible as the shear connections are inaccessible. Traditional vibration-based methods have been generally used for the SCC beams damage detection. Xia et al. (Xia et al. 2007) showed that the global vibration parameters of SCC beam structures such as natural frequencies, mode shapes, and the derivations of mode shapes are not sensitive to the interface slip and do not apply to this type of local damage (Housner et al. 1997; Ren and De Roeck 2002). Thus, developing innovative methods to identify damage from the interface shear slip is essential for beam bridges.

There are two main strategies to locate damage in composite beam bridges (Sun et al. 2020; Ren and De Roeck 2002). The first strategy is known as model-based methods, in which a finite element (FE) model of the structure is developed and updated to represent the baseline for the real structure. Then, the response of the structure in the damaged state is compared with the undamaged state to derive knowledge about the damage location and severity. The second strategy is rooted in analysing the structural response using signal processing techniques. In these methods, the location of local damage is tracked by peaks in signals. To identify the damage, the signals are decomposed into constructive narrow-banded components by means of some time-frequency signal decomposition techniques such as wavelet transform (WT) (Yan and Ren 2013; An et al. 2015), empirical mode decomposition (EMD) (Poskus et al. 2018; Roveri and Carcaterra 2012), or variational mode decomposition (VMD) (Li et al. 2018). Data-driven methods are also employed to analyse such signals by machine learning (ML) algorithms.

In the response-based SHM methods, the most significant and widely used signal processing technique is EMD (Mousavi et al. 2021). In this technique, the cubic spline is employed to interpolate between the average of the peaks and troughs, and these curves, known as Intrinsic Mode Functions (IMFs), are recursively subtracted from the signal. EMD is effective at maintaining the non-linear response of the bridge against load where the local damage exists. These non-linear responses are reflected in the signal's higher frequency bands which are more sensitive to damage (Xu and Chen 2004; Meredith et al. 2012). Roveri and Carcaterra (Roveri and Carcaterra 2012) employed the EMD and instantaneous frequency (IF) to detect open cracks in a bridge beam. In a study by Cheragi and Taheri (Cheraghi and Taheri 2007), damage indices are introduced by integrating EMD and using the Fast Fourier Transform (FFT) to identify stiffness reduction in a vibrating pipe. An FE model of the structure was developed for the damaged and undamaged states of the structures, and the first IMF was observed to extract the damage quantity and location.

Although the higher frequency bands are often used for damage detection, obtaining those frequencies is not easy in practice. Besides, the majority of EMD studies used a baseline model (undamaged) or noise was not considered. To capture the non-linear part of a time-history signal, several signal processing techniques have been developed and used in recent years (Altan et al. 2019; Dragomiretskiy and Zosso 2014). In the following sections, the drawbacks of the EMD signal processing technique are described, and then VMD is proposed as an alternative to EMD. The VMD is an efficient signal processing tool, extensively used for fault detection in mechanical systems (Chen et al. 2019b; Wang et al. 2019). In this paper, a response-based damage identification method is presented using the VMD of shear slip measurements of a beam bridge subjected to the local stiffness reduction.

SIGNAL PROCESSING TECHNIQUES

Empirical mode decomposition (EMD)

The EMD is an empirical decomposition algorithm used to decompose a non-linear/non-stationary signal into its IMFs or oscillation modes (Huang et al. 1998). In a non-stationary signal, frequency is inconsistent within amplitude and can be adjusted. Although IMFs obtained from the EMD analysis can be non-stationary, each IMF is narrowband and involves one mode of oscillation. This is an identical feature to the traditional linear analysis. Fig.1 shows the flowchart of the EMD algorithm in terms of a signal X(t).

Several authors have utilized the EMD for structural damage identification due to its effectiveness in decomposing non-linear/non-stationary signals into its components (Cheraghi and Taheri 2007; Pines and Salvino 2006; Xu and Chen 2004). However, the EMD has some drawbacks in signal decomposition. For example, it was shown that the change in IFs cannot be detected by the EMD when the derived IMFs include wide-band frequencies. To deal with this issue, Yang (Yang 2008) proposed an improved Hilbert-Huang Transform (HHT) for decomposing a signal into mono-component parts. Besides, the sensitivity of the EMD against uncertainties such as sampling and noise effects has been raised by (Rilling and Flandrin 2009) and to deal with these shortcomings, a novel approach called variational mode decomposition (VMD) has been recently proposed (Dragomiretskiy and Zosso 2014). The approach is a generalization of the classic Wiener filter and is useful for the adaptive decomposition of a signal into its components. Hence, compared to the EMD, the VMD is completely non-recursive.

Variational mode decomposition (VMD)

The VMD is an efficient technique to decompose a real-valued signal $X(t)$ into its components. In this technique, the criteria for a mode that is evaluated as an IMF is somewhat different (Gilles 2013). Thus, an IMF is defined as an Amplitude-Modulated-Frequency-Modulated (AM-FM) sinusoid. The AM-FM has the characteristics such as the phase corresponding to an IMF is a non-decreasing function, the envelope of the IMF is non-negative, and both the envelope and the IF corresponding to an IMF change slower than the phase. Therefore, the updated IMF, $u_k(t)$ can be written as:

$$u_k(t) = A_k(t)\cos(\phi_k(t)), \tag{1}$$

where $A_k\ (t)$ and $\phi_k\ (t)$ are the instantaneous amplitude and phase, respectively. The updated IMF is moderately more restrictive than the original IMF and hence, a mode will have a small frequency range that complies with the mono-component signal concept. Fig.2 shows the VMD algorithm and its steps. To implement the algorithm, two extra terms are added to the main algorithm to resolve the optimisation problem including (a) a quadratic penalty at finite weight, and (b) a Lagrangian multiplier to strictly enforce the constraint. The first term could further undertake the achievement of convergence if noise exists in the signal. Therefore, the algorithm has the following key feature:

1. To reduce the effect of noise in the decomposed IMFs, a quadratic penalty term of higher values α is defined. Although increasing α leads to a decrease in the bandwidth and subsequently a decrease in the accuracy, the centre frequency of each mode is captured. The loss of accuracy reduces noise effects from the IMFs leading to a less noisy version of

the original signal when all the extracted IMFs are cumulated.

2. To select the number of modes K which are needed to signal decomposition. Unlike the EMD, the VMD enables the decomposition of a signal into an arbitrary number of IMFs. To the authors' best knowledge, the structural system and its measured features play a significant role in making a reasonable decision on the optimum numbers of IMFs. The EMD, however, recursively decomposes a signal which leads to difficulty in controlling the decomposition steps, which may result in over-decomposing a signal into abundant IMFs. This could result in missing information, particularly when noise exists in the signal.
3. To control the relative error in the re-constructed modes, a convergence level ϵ is introduced. It is worth noting that when ϵ values are small, the decomposition is essentially independent of the value chosen for ϵ.

In this paper, VMD is used to decompose the signals representing the interlayer slip of the composite beam under study into two modes. The centre frequency of the second mode, which is of higher centre frequency, is then taken as Damage Sensitive Feature. The VMD is a parametric signal decomposition algorithm, and, therefore, there are some parameters that are required to be specified prior to running the decomposition (Zosso 2021). These parameters and their recommended values for the purpose of this paper are listed in Table 1. Note that the settings are identical for both numerical and experimental studies.

The main aim of signal decomposition is considered to isolate the high-frequency content of the slip signal. This is only made possible by controlling the number of decompositions in the VMD settings. As such, the number of decomposed IMFs was set to 2 to derive two main IMFs, which are: (1) the ascending long-term trend in the signal which reflects the gradual increase of slip recorded at the sensors, and (2) a semi-dynamic pattern in the slip signal that reflects the dynamic nature of the slip at the sensors even when the load is statically applied.

The quadratic penalty term is a parameter that controls the extent of denoising introduced to the decomposition process. The over-denoising of the signal will likely compromise the process of extracting information from a higher mode. The reason is that the proposed method seeks to identify the centre frequency of the second mode (a mode with a high centre frequency) as DSF, which can be over-smoothed if α is set at a large value. Therefore, α was set to 100 to introduce slight denoising in the decomposition process. In case this might seem case dependent, the authors recommend setting the time step τ to a very small number such as 0.1 (as recommended by the proposers of the VMD (Wang et al. 2015)) to avoid denoising. This will subsequently make the computer program ignore the effect of the denoising factor α.

The tolerance parameter is the threshold that controls convergence in the algorithm. A value of 10^{-7} is a sufficiently small value for controlling the convergence of the algorithm, where any smaller value would only increase the timing of the process while not improving the results. The centre frequency initialiser is a parameter that determines the initial guess for the centre frequencies of the to-be-identified IMFs. It can take different values of 0 (indicating zero initialization), 1 (indicating uniform initialization, and 2 (indicating random initialization). It has been reported that the way of initializing the centre frequency has no significant impact on the decomposition results (Zosso 2021). Therefore, 0 was selected as the initial guess for the centre frequency of the two IMFs.

Note that the first mode is ideal to be kept in the same format as the original signal to avoid mode mixing as much as possible. The parameter τ is a Boolean parameter in the VMD settings that enforces the centre frequency of the first IMF to be either zero ($\tau = 1$) or otherwise ($\tau = 0$). Therefore, to keep the first mode as much similar as possible to the original signal, DC was set to 1. For further information about the ways of specifying the settings of the VMD, the readers are referred to (Mousavi et al. 2021; Mousavi and Gandomi 2021b; Mousavi and Gandomi 2021a).

EXPERIMENTAL SETUP

Bridge model

A laboratory-scale bridge model consisting of SCC beams is considered for the experimental studies. The bridge was designed according to Australian standards (Australia 2002; Australia 2003) and consists of three independent spans; a 2m cantilever beam on the left-hand side (LHS), a 6m span in the middle (main span), and a 2m span on the right-hand side (RHS). The end-to-end length of the bridge is 10m with 0.1m depth reinforced concrete slabs seated on the top of two parallel UC-150-23 steel girders. In this paper, the 6m main span is used to study its behaviour under loading, and damage scenarios are simulated by the removable shear connectors. Concrete grade 40 was used to construct slabs and connected to the steel girders by shear connectors marked as bolt SC32 with 30mm centre to centre spacing. The Modulus of elasticity and density of the concrete and the steel are E_c=32000 MPa, ρ_c=2700 kg/m^3, E_s=210000 MPa, ρ_s=7800 kg/m^3, respectively.

Seven slip sensors were installed equally along the half of one girder. Although the maximum shear slips between the composite layers generally occur at the ends of the span (at supports), sensors were set up along half of a beam for accurate assessment of damage in different locations. The shear connectors (bolts) could be unscrewed to simulate damage and hence induce shear links' failure, and redone to form the intact bond. 13 bolts were screwed into tube nuts embedded in the concrete slab corresponding to the intact beam on each side of a steel girder top flange. Bolts were numbered from the RHS to LHS. Fig.3a shows the bridge model at the laboratory indicating the span of interest with a discontinuous slab which allows it to independently act on other slabs under loading. Fig.3b shows the bolts and their tube nuts embedded (Fig.3c) in the main concrete slab during construction.

Experimental set-up

The experimental study was carried out on the bridge by monitoring its shear connections behaviour in terms of shear slip when an external load is applied. Ultra-flat Industrial Potentiometer Membrane (UIPM) slip sensors were used to measure shear slip between the concrete slab and steel girder. The measurement range of the sensor is up to 47mm (Sadeghi et al. 2021b). Seven slip sensors were evenly installed along the half of a steel girder and connected to 7-channels (in one Module) in the National Instrument data acquisition system. Time-domain data (Relative displacements between two layers over time) were collected using LabVIEW data collection software and multiplied with a specific calibration coefficient (Sadeghi et al. 2021b). Fig.4 shows the locations of the slip sensors on the bridge. Three incremental load cases including 375, 750, and 1100 kgs, were considered for intact, single and double damage scenarios to measure shear slip of the intact and damaged bridge. The shear slips of the intact bridge were measured as the benchmark data. The single damage scenario was defined by unscrewing the bolts in the second row (both sides of the steel girder), and the shear slips of the bridge were recorded. Then, the double damage scenario was simulated by unscrewing the bolts of the second and fifth rows.

Benchmark shear slip

To collect benchmark slip data, all shear connectors were tightened with standard torque for 30mm bolts, and then the three load cases were separately applied at the mid-span of the bridge. The quantity of the applied loads was less than 40 percent of the bridge load-bearing capacity to avoid either visible cracks or failure. The purpose of this research is to detect small damage to the composite interface before a catastrophic condition occurs. Fig.5 shows the load application approaches in the laboratory which were established by placing concrete blocks at the main span. Only shear slip data were used when all concrete blocks (full loading) were equally put for each load case at the mid-span. This is to avoid the torsion effect on the data which may appear by loading on one of the beams at mid-span. An overall time of 1000 seconds was enough for each load case in the interval of full loading to become stable.

Fig.6 shows the shear slip of the bridge for three incremental cases collected from seven sensors labelled 1 to 7 from the support to the mid-span. The first, second and third load increments (cases) are marked up as 1, 2 and 3, respectively. The minor movements of the composite layers before case 1 in the unloaded area could be due to the self-weight of the structure. The visible elevations in the interval of 0 to 1, 1 to 2, and 2 to 3 are due to the collision of putting concrete blocks for each case. But full loading data, which is the last record, are considered as the maximum slip for each load case. The straight lines show the times spent to allow the bridge to become stable for the next loading.

Table 2 shows the maximum shear slip location recorded by a specific sensor for each load case. maximum slips of 0.02mm (recorded by Sensor 5 located at the loading zone), 0.09mm (recorded by Sensor 2), and 0.12mm (recorded by Sensor 1) were respectively recorded for the first, second, and third load cases. There was no slip at the mid-span where loads were applied and Sensor 7 was installed. The shear slip was expected to be zero at the mid-span and maximum at the end supports. This assumption was achieved in the third load case where the quantity of the load was enough to compel the bridge for having a visible deflection.

Scenario 1: Single damage

The single damage scenario was defined by unscrewing the second row (both sides of the steel top flange) of bolts, as shown in Fig.7. The bridge was subjected to the three incremental load cases and shear slip data were recorded from the slip sensors. Fig.8 shows the shear slip of the bridge due to the three incremental load cases, which are recorded from slip sensors. Maximum shear slips for the load cases and their alterations due to the damage are presented in Table 2. Maximum slips of 0.04mm (recorded by Sensor 2), 0.15mm (recorded by Sensor 2), and 0.19mm (recorded by Sensor 1) were respectively recorded for the first, second and third load cases. In this case, also, there is no slip at the mid-span where loads were applied and Sensor 7 was installed.

Scenario 2: Double damage

Double damage is defined by unscrewing bolts at two different locations including the second and fifth rows (both sides of steel top flange), as shown in Fig.9. The same load cases in Sections 3.4 and 3.5 were applied to the bridge and shear slip data were collected from the slip sensors. Fig.10 depicts the shear slip of the bridge subjected to the load cases. Maximum shear slips due to the double damage are presented in Table 2. For first and second load cases, maximum slips of 0.14mm and 0.22mm were recorded by Sensor 2. A maximum slip of 0.32mm for the third load case was recorded at Sensors 1 and 2. In this case, also, there is no slip at the mid-span at the location of load application and Sensor 7.

FINITE ELEMENT MODELLING

A finite element (FE) model of the SCC beam was developed based on the assumptions and formulations presented by Sadeghi et al. (Sadeghi et al. 2021a; Sadeghi 2021) in which steel beam and concrete slab are modeled as Euler-Bernoulli beam elements which are coupled by a deformable shear connection distributed at their interface (Girhammar and Gopu 1993; Salari et al. 1998). The shear connection was assumed to be a uniform spring enabling longitudinal slip between upper and lower elements (Wang 1998). Shear slip g at the interface is calculated using the following equation:

$$g = u_c(x) - u_s(x) + h\partial_x \upsilon(x) \tag{2}$$

Damage index

The stiffness parameter of a structure can be used as an indicator because damage causes changes in the stiffness which is reflected in the structural response. Here, reduced stiffness by damage in any composite component is defined by scalar variables α_i $(i = 1, 2, \ldots, n)$, in which i is an element and n is the total number of elements. Thus, a damage index is introduced by the element stiffness reduction as:

$$\mathbf{K}_e = (1 - \alpha)\hat{\mathbf{K}}_e \tag{3}$$

where $\mathbf{K}_e$ is the damaged element stiffness matrix, $\hat{\mathbf{K}}_e$ is the undamaged element stiffness matrix and α is the value of the damage index. Eq.(3) is extended to three damage indices of α_s, α_c and α_b for steel, concrete and interface elements, respectively. These indices allow consideration of the three types of failure modes including steel beam failure, concrete crushing, and shear failure of the studs (Sadeghi et al. 2021a). An element without damage has a zero index value ($0 \leq \alpha_c, \alpha_s, \alpha_b \leq 1$).

Damage scenarios and shear slips

Numerical tests were conducted on the developed FE model of the composite beam by applying a point load of $P = 10000$ N at its mid-span and the relative displacements were measured from different points along the beam. To simulate real-world structural conditions and uncertainties, a median white noise of 5% was applied to the data in any intact and damaged scenarios. The results obtained from the damaged states are compared with the intact state for the purpose of damage identification. Figure 11 shows the measured data from the intact FE model of the beam through a time interval of 1000 seconds. Since a simply supported beam with a roller at the LHS and pin at the RHS are considered, maximum relative displacement (shear slip) is obtained in Sensor 1 where roller support allows the beam to move in the horizontal direction. The second maximum displacement is recorded by Sensor 2 which is close to the left support. Sensor 4, located in the middle of the beam, has no obvious changes, but some minor fluctuation can be due to the point load position.

The FE model of the beam was used to simulate three scenarios of the health condition of the beam, including intact, single damage, and double damage. For all damage scenarios, 90% damage was simulated on finite elements of the composite beam interface at the location of bolt number 2 for single damage and bolts number 2 and 5 for double damage. Figures 12 and 13 show the results of the FE simulation in terms of relative displacement and time.

In a single damage scenario, no changes in shear slip data are observed for Sensor 4 located in the mid-span. Sensors 1 and 2, which are in the LHS and close to the roller support, show maximum shear slips and increments in shear due to the existence of damage in bolt number 2. Other sensors have minor increases compared to the intact data, which are due to the instability and non-linearities of composite action affected by damage at the interface (Fig.12). In the double damage scenario, in addition to continuous increments in Sensors 1 and 2, observable increases in Sensor 5 in the location of damage and Sensor 7 in the RHS support occurred. Sensor 4 in the mid-span shows constant values, and Sensors 5 and 6 in the LHS and RHS of the mid-span have the smallest changes and fluctuations. The results obtained from the numerical modelling show damage at the composite interface affects both composite action and the shear slip data. Although changes in the shear slip due to damage are minor, the overall behaviour of the composite beam and its load-bearing capacity are influenced. Therefore, more accurate and robust signal processing techniques are needed to track and identify such minor changes.

RESULTS AND DISCUSSION - SIGNAL PROCESSING AIDED DAMAGE DETECTION

Results of the FE model

The VMD is employed to decompose the recorded signals of the composite beam's interlayer shear slips through analysis of the first two IMFs. The centre frequency of the IMF with a higher centre frequency (the second IMF) is considered sensitive to damage. This is mainly due to the fact that damage is expected to increase the fluctuation of the slip at a support location as the load is gradually and incrementally introduced to the beam. The proposed method requires baseline data obtained from the intact structure. In the FE model, shear slips are obtained from seven sensors (points) evenly spaced along the beam. The VMD algorithm is then applied to the signal obtained from each sensor. Table 3 presents the centre frequency of the IMFs for undamaged and two damage scenarios. The results indicate that the centre frequency of the IMF2 signals increases as damage progresses in the beam. However, it is worth noting that the results for all the sensors are identical. This could be owing to not including the friction effect in the FE model of the composite beam. The friction could have a significant effect on the interlayer shear slip at one cross-section while damage may occur at non-adjacent cross-sections. In this condition, more shear slip is expected to occur at the cross-section which is close to the defected cross-section, and the lesser shear slip occurs at farther cross-sections from the defect zone. However, the friction does not affect the interlayer slip when there is no vertical motion (uplift effect) between two layers of the composite beam (Andrews et al. 1996). In this paper, the FE modelling is based on two Euler-Bernoulli beam elements with just interlayer slip and transverse displacements between two layers were neglected (no uplift) due to small displacements.

To further investigate the damage detection capability of the IMF signals obtained from decomposition of the shear slip data using the VMD algorithm, the Welch power spectral densities (WPSD) of the IMFs are drawn in a plot. Fig.14 shows the IMF2 signals obtained from the decomposition of the shear slip data at Sensor 1 and their corresponding WPSD (see pwelch syntax in MATLAB), in all the introduced damage scenarios including undamaged (U), single damage (first scenario - D1), and double damage (second scenario - D2).

It is observable in the plots that the energy of the frequency content regarding the IMF2 signals increases as damage progresses in the FEM of the beam. Besides, a slight shift is noted in the energy concentration of the frequency content towards the right as damage progressed in the model. Here, the EMD algorithm, a conventional signal processing tool, described in Section 2 is intended to apply to the shear data to make a comparison with the VMD results. Fig.15 shows IMFs 1 and 2 calculated by the VMD algorithm for the signal obtained from Sensor 1 for the undamaged scenario.

Although the VMD decomposed the signals properly, the EMD was not able to decompose the shear slip data.

Results of the experimental model

The proposed VMD method is examined on the results of the test conducted on the experimental model presented in Section 3 which are in terms of three damage scenarios including undamaged, single (unscrewing the second row of bolts) and double damage (unscrewing the second and fifth row of bolts). It is worth noting that the settings of the VMD are the same as the numerical model in Section 4. The VMD is employed to decompose the shear slip signals of the composite beam through the analysis of two IMFs assuming that the centre frequency of the IMF with a higher centre frequency is sensitive to damage. In the experimental set-up, shear slips are obtained from seven sensors evenly situated along the half of the beam from the support to mid-span. The VMD algorithm is then applied to the signal obtained from each sensor. Since the slip at one point can well affect the amount of slip sensed at an adjacent sensor. Therefore, the proposed method may be used to identify damaged shear connectors one at a time through the following procedure:

1. Find the most plausible defective shear connector.
2. Fix the identified damaged shear connector.
3. Repeat the experiment to see whether or not there exists any other significant damage at the location of another sensor.
4. Repeat steps (2) and (3) until no other significant changes to the proposed DSF can be identified.

Table 4 shows the centre frequency of the IMFs for undamaged and damage scenarios. The results indicate that the centre frequency of the IMF2 signals changes as damage progresses in the beam.

Based on the results presented in Table 3, the following equation is introduced as the damage sensitive feature (DSF):

$$\text{DSF} = \left|\omega_2^d - \omega_2^h\right| \tag{4}$$

where ω_2^d and ω_2^h are the centre frequencies of the second IMF obtained from the decomposition of the interlayer shear slip signals of the damaged and intact beam, respectively. Thus, the proposed DSF has been calculated for undamaged and damage scenarios as presented in Fig.16. The results indicate that the proposed DSF obtained larger at the sensors deployed near the damage site. For single damage, the value of DFS clearly indicates the location of damage in Sensor 2. Although the damage in the location of Sensor 2 is apparent in the DFS value for the double damage scenario, there is a relative error in detecting damage at Sensor 5 which is appeared in Sensor 4. The error of identification in this scenario is predictable because Sensor 5 is close to the mid-span where the load was applied and the shear slip changes are very small.

Fig.17 shows IMFs 1 and 2 calculated by the VMD algorithm for the signal obtained in Sensor 1 for the undamaged scenario of the experimental model. For comparison, the EMD algorithm is employed to decompose the same signal. Fig.18 shows nine first IMFs obtained from the decomposition of the shear slip signal by the EMD algorithm. The results show that employing the EMD has not been successful in the decomposition of the shear slip signals useable for damage detection. This is due to the signal over-decomposition and mode-mixing which are the inherent drawbacks of the EMD algorithm. For the purpose of damage detection using the shear slip parameter, the main objective of the decomposition is to extract an IMF with a high-frequency content that can be corresponded to the abnormal fluctuation of the shear slip signal at a particular location of the beam. In this study, the preference is to decompose a signal into two IMFs with high-frequency contents and information rather than over-decomposing the signal. The VMD complies with the requirement by characterising the number of decompositions. However, the EMD algorithm decomposes empirically a signal into as many IMFs as possible without considering the frequency content of the signal. This misleads the damage detection process as the signal over-decomposition could result in losing information about the damage state of the structure. Besides, information about the damage existence in the shear slip is more likely to spread across various IMFs through the EMD analysis because of the mode-mixing problem of the EMD algorithm.

Moreover, since the damage exists at the location of Sensor 2 in both the single and double damage scenarios, the shear slip signals obtained from Sensor 2 are considered for further analysis by extracting the WPSDs of the IMF2 obtained from the VMD algorithm. Fig.19 shows the results of WPSD analysis for the undamaged and damaged scenarios. The results indicate that the energy of the frequency content of the signal obtained from Sensor 2 is increasing as damage progresses on the beam. This phenomenon is also experienced in the results obtained from the sensors on non-defective locations on the beam. This is due to the effect of damage in the composite section which is reflected in the global behaviour of the beam and consequently in the shear slip at different locations. However, the variations of WPSDs are more sensitive at the location of damage in Sensor 2 indicating a damage index could be drawn from the WPSD of IMF2 of the shear slip.

CONCLUSION

In this paper, a novel approach for damage detection of SCC beams has been presented based on the VMD of shear slip data. The experimental set-up was established on an SCC beam bridge and shear slip data were acquired from the shear slip sensors UIPM for the undamaged and damaged states of the model. The damage on the composite interface was simulated by unscrewing the second row of shear connectors for the single damage scenario and the second and fifth rows of shear connectors for the double damage scenario. Then, the structure was subjected to various incremental loads and shear slip data were recorded. Besides, an FE model was developed considering steel beam and concrete slab as Euler-Bernoulli beam elements which were coupled by a deformable shear connection distributed at their interface. The shear connection was assumed to be a uniform spring enabling longitudinal slip between upper and lower elements. The numerical tests were conducted on the FE model by applying a point load at the mid-span of the bridge and the shear slips were measured from different points along the beam. To simulate real-world structural conditions and uncertainties, a median white noise of 5% was applied to the data in any intact and damaged scenarios. Although the same damage scenarios were considered for the experimental and FE models, the sensors were spread equally along the whole span of the FE model and the half span of the experimental model. The results obtained from the undamaged and damaged states of both models were employed for the damage detection. The VMD algorithm was used to decompose shear slip data into IMFs and the peaks in the centre frequencies of IMF2 were used for the damage detection. The traditional signal processing tool EMD was also employed to extract IMFs from shear slip data to compare with those obtained from the VMD. The findings obtained from the signal processing-aided damage detection are listed below:

- The noise effect on the decomposed IMFs obtained from the VMD algorithm has been eliminated by increasing the quadratic penalty term of higher values and then, the centre frequency of each mode has been captured. This has resulted in obtaining a reduced noisy version of the original signal when all the extracted IMFs are cumulated.
- The EMD has recursively decomposed the signals which resulted in missing information of each IMFs in both numerical and experimental cases. However, the VMD has enabled the decomposition of a signal into two arbitrary numbers of the IMFs with higher frequency content in the second mode.
- The results of the numerical study have indicated that the centre frequency of the IMF2 signals increases identically in all sensors as damage progresses in the beam.
- The WPSDs of IMFs were calculated to further investigate the changes in the centre frequencies of IMFs signals obtained from the VMD algorithm was carried out. It has been shown that the energy of the frequency content regarding the IMF2 signals increased as damage progressed in the FEM of the beam.
- The results obtained from the experimental study have shown that the IMF2, which has the higher centre frequency contents, changed as damage progressed in the beam. Thus, the variation in the centre frequency of the IMF2 has been taken as a damage sensitive feature. Besides, the variations of WPSDs have been more observable at the damage location indicating a damage index in the WPSDs of IMF2.
- The DSF has been defined based on the centre frequencies of the IMF2s in undamaged and damaged states. The results have shown that although the DSF has a greater value at the damage zone in Sensor 2 for the single damage scenarios, there has been a relative error in detecting double damage in Sensor 5 location. The identification error in this scenario is

predictable as Sensor 5 is close to the mid-span, and the friction effect and uncertainties of the experimental condition can cover the signal's abnormal changes.

- In summary, the EMD has been unable to detect damage from changes in the shear slip signals. However, the proposed VMD based method has been reliable in damage detection of the composite beams as it reveals peaks in curves and changes in the energy of centre frequencies of shear slip data.

DATA AVAILABILITY STATEMENT

Some or all data, models, or code generated or used during the study are proprietary or confidential in nature and may only be provided with restrictions.

AUTHOR CONTRIBUTION

Conceptualization, F.S., M.M., and A.G.; Data curation, F.S. and M.M.; Formal analysis, F.S. and M.M.; Investigation, F.S. and M.M.; Methodology, F.S. and M.M.; Supervision, A.G., B.S., and M.R.; Validation, A.G., B.S., and M.R.; Writing–original draft, F.S. and M.M.; Writing–review & editing, F.S., M.M., A.G., X.Z., B.S., and M.R.

REFERENCES

Altan, A., Karasu, S., and Bekiros, S. (2019). "Digital currency forecasting with chaotic meta-heuristic bio-inspired signal processing techniques." *Chaos, Solitons & Fractals*, 126, 325–336.

An, Y., Chatzi, E., Sim, S.-H., Laflamme, S., Blachowski, B., and Ou, J. (2019). "Recent progress and future trends on damage identification methods for bridge structures." *Structural Control and Health Monitoring*, 26(10), e2416.

An, Y., Spencer Jr, B., and Ou, J. (2015). "A test method for damage diagnosis of suspension bridge suspender cables." *Computer-Aided Civil and Infrastructure Engineering*, 30(10), 771–784.

Andrews, K. T., Shillor, M., and Wright, S. (1996). "On the dynamic vibrations of an elastic beam in frictional contact with a rigid obstacle." *Journal of elasticity*, 42(1), 1–30.

Australia, S. (2002). "Structural design actions part 1 – permanent, imposed and other actions." *Report No. AS/NZS 1170.1:2002*, nd.

Australia, S. (2003). "Composite structures: simply-supported beams." *Report No. AS/NZS 2327.1: 2003*, nd.

Chen, J., Zhang, H., and Yu, Q.-Q. (2019a). "Static and fatigue behavior of steel-concrete composite beams with corroded studs." *Journal of Constructional Steel Research*, 156, 18–27.

Chen, X., Yang, Y., Cui, Z., and Shen, J. (2019b). "Vibration fault diagnosis of wind turbines based on variational mode decomposition and energy entropy." *Energy*, 174, 1100–1109.

Cheraghi, N. and Taheri, F. (2007). "A damage index for structural health monitoring based on the empirical mode decomposition." *Journal of Mechanics of Materials and Structures*, 2(1), 43–61.

Dilena, M. and Morassi, A. (2004). "Experimental modal analysis of steel concrete composite beams with partially damaged connection." *Journal of Vibration and Control*, 10(6), 897–913.

Dragomiretskiy, K. and Zosso, D. (2014). "Variational mode decomposition." *IEEE transactions on signal processing*, 62(3), 531–544.

Gilles, J. (2013). "Empirical wavelet transform." *IEEE transactions on signal processing*, 61(16), 3999–4010.

Girhammar, U. A. and Gopu, V. K. (1993). "Composite beam-columns with interlayer slip—exact analysis." *Journal of Structural Engineering*, 119(4), 1265–1282.

Ho, S. C. M., Ren, L., Labib, E., Kapadia, A., Mo, Y.-L., Li, H., and Song, G. (2015). "Inference of bond slip in prestressed tendons in concrete bridge girders." *Structural Control and Health Monitoring*, 22(2), 289–300.

Housner, G., Bergman, L. A., Caughey, T. K., Chassiakos, A. G., Claus, R. O., Masri, S. F., Skelton, R. E., Soong, T., Spencer, B., and Yao, J. T. (1997). "Structural control: past, present, and future." *Journal of engineering mechanics*, 123(9), 897–971.

Huang, N. E., Shen, Z., Long, S. R., Wu, M. C., Shih, H. H., Zheng, Q., Yen, N.-C., Tung, C. C., and Liu, H. H. (1998). "The empirical mode decomposition and the hilbert spectrum for nonlinear and non-stationary time series analysis." *Proceedings of the Royal Society of London. Series A: mathematical, physical and engineering sciences*, 454(1971), 903–995.

Li, H., Dong, S., El-Tawil, S., and Kamat, V. R. (2013). "Relative displacement sensing techniques for postevent structural damage assessment.” *Journal of Structural Engineering*, 139(9), 1421–1434.

Li, J. and Hao, H. (2016). “Health monitoring of joint conditions in steel truss bridges with relative displacement sensors.” *Measurement*, 88, 360–371.

Li, J., Hao, H., Fan, K., and Brownjohn, J. (2015). “Development and application of a relative displacement sensor for structural health monitoring of composite bridges.” *Structural Control and Health Monitoring*, 22(4), 726–742.

Li, Y., Li, G., Wei, Y., Liu, B., and Liang, X. (2018). “Health condition identification of planetary gearboxes based on variational mode decomposition and generalized composite multi-scale symbolic dynamic entropy.” *ISA transactions*, 81, 329–341.

Meredith, J., González, A., and Hester, D. (2012). “Empirical mode decomposition of the acceleration response of a prismatic beam subject to a moving load to identify multiple damage locations.” *Shock and Vibration*, 19(5), 845–856.

Mousavi, M. and Gandomi, A. H. (2021a). “Prediction error of johansen cointegration residuals for structural health monitoring.” *Mechanical Systems and Signal Processing*, 160, 107847.

Mousavi, M. and Gandomi, A. H. (2021b). “Structural health monitoring under environmental and operational variations using mcd prediction error.” *Journal of Sound and Vibration*, 512, 116370.

Mousavi, M., Holloway, D., Olivier, J., and Gandomi, A. H. (2021). “Beam damage detection using synchronisation of peaks in instantaneous frequency and amplitude of vibration data.” *Measurement*, 168, 108297.

Nguyen, Q.-H., Hjiaj, M., and Guezouli, S. (2011). “Exact finite element model for shear-deformable two-layer beams with discrete shear connection.” *Finite elements in analysis and design*, 47(7), 718–727.

Nie, J. and Cai, C. S. (2003). “Steel–concrete composite beams considering shear slip effects.” *Journal of Structural Engineering*, 129(4), 495–506.

Pines, D. and Salvino, L. (2006). “Structural health monitoring using empirical mode decomposition and the hilbert phase." *Journal of sound and vibration*, 294(1-2), 97–124.

Poskus, E., Rodgers, G. W., Zhou, C., and Chase, J. G. (2018). "Damage identification for hysteretic structures using a mode decomposition method." *Computer-Aided Civil and Infrastructure Engineering*, 33(2), 97–109.

Ren, W.-X. and De Roeck, G. (2002). "Structural damage identification using modal data. i: Simulation verification." *Journal of Structural Engineering*, 128(1), 87–95.

Rilling, G. and Flandrin, P. (2009). "Sampling effects on the empirical mode decomposition." *Advances in Adaptive Data Analysis*, 1(01), 43–59.

Roveri, N. and Carcaterra, A. (2012). "Damage detection in structures under traveling loads by hilbert–huang transform." *Mechanical Systems and Signal Processing*, 28, 128–144.

Sadeghi, F. (2021). "Structural health monitoring of composite bridges by integrating model-based and data-driven methods.

Sadeghi, F., Li, J., and Zhu, X. (2020). "A steel-concrete composite beam element for structural damage identification." *International Journal of Structural Stability and Dynamics*, 20(10), 2042015.

Sadeghi, F., Yu, Y., Zhu, X., and Li, J. (2021a). "Damage identification of steel-concrete composite beams based on modal strain energy changes through general regression neural network." *Engineering Structures*, 244, 112824.

Sadeghi, F., Zhu, X., Li, J., and Rashidi, M. (2021b). "A novel slip sensory system for interfacial condition monitoring of steel-concrete composite bridges." *Remote Sensing*, 13(17), 3377.

Salari, M. R., Spacone, E., Shing, P. B., and Frangopol, D. M. (1998). "Nonlinear analysis of composite beams with deformable shear connectors." *Report No. 10*.

Sun, L., Shang, Z., Xia, Y., Bhowmick, S., and Nagarajaiah, S. (2020). "Review of bridge structural health monitoring aided by big data and artificial intelligence: From condition assessment to damage detection." *Journal of Structural Engineering*, (5), 04020073.

Vasdravellis, G. and Uy, B. (2014). "Shear strength and moment-shear interaction in steel-concrete composite beams." *Journal of Structural Engineering*, 140(11), 04014084.

Wang, X., Gao, J., Wei, X., Song, G., Wu, L., Liu, J., Zeng, Z., and Kheshti, M. (2019). "High impedance fault detection method based on variational mode decomposition and teager–kaiser energy operators for distribution network." *IEEE Transactions on Smart Grid*, 10(6), 6041–6054.

Wang, Y., Markert, R., Xiang, J., and Zheng, W. (2015). "Research on variational mode decomposition and its application in detecting rub-impact fault of the rotor system." *Mechanical Systems and Signal Processing*, 60, 243–251.

Wang, Y. C. (1998). "Deflection of steel-concrete composite beams with partial shear interaction." *Journal of Structural Engineering*, 124(10), 1159–1165.

Xia, Y., Hao, H., and Deeks, A. J. (2007). "Dynamic assessment of shear connectors in slab–girder bridges." *Engineering Structures*, 29(7), 1475–1486.

Xu, Y. L. and Chen, J. (2004). "Structural damage detection using empirical mode decomposition: experimental investigation." *Journal of engineering mechanics*, 130(11), 1279–1288.

Yan, W.-J. and Ren, W.-X. (2013). "Use of continuous-wavelet transmissibility for structural operational modal analysis." *Journal of Structural Engineering*, 139(9), 1444–1456.

Yang, W.-X. (2008). "Interpretation of mechanical signals using an improved hilbert–huang transform." *Mechanical Systems and Signal Processing*, 22(5), 1061–1071.

Zhang, Q., Jia, D., Bao, Y., Dong, S., Cheng, Z., and Bu, Y. (2019). "Flexural behavior of steel-concrete composite beams considering interlayer slip." *J. Struct. Eng*, 145(9), 04019084.

Zosso, D. (Retrieved 2021). "Variational mode decomposition, matlab central file exchange, <https://www.mathworks.com/matlabcentral/fileexchange/44765-variational-mode-decomposition>.

List of Tables

TABLE 1. Parameters of the VMD and their selected values in this paper.

Description	Nomenclature	Specified value
Number of IMFs	K	2
Denoising factor	α	100
Time interval	τ	0
Convergence threshold	ϵ	10^{-7}
Center frequency initialiser	$init$	0
Boolean parameter	DC	1

TABLE 2. The maximum shear slips of the bridge for different load cases and damage scenarios.

Damage scenario	Load Case 1		Load Case 2		Load Case 3	
	Slip (mm)	Sensor	Slip (mm)	Sensor	Slip (mm)	Sensor
Benchmark	0.02	5	0.09	2	0.12	1
Scenario 1	0.04	2	0.15	2	0.19	1
Scenario 2	0.14	2	0.22	2	0.32	1& 2

TABLE 3. The centre frequency of the IMF2 signals obtained from the decomposition of the interlayer slip signals for the damage scenarios, U, D1, and D2 regarding the FEM of the beam.

Sensors No.	1	2	3	4	5	6	7
Undamaged	0.0817	0.0817	0.0817	0.0817	0.0817	0.0817	0.0817
Scenario 1	0.093	0.093	0.093	0.093	0.093	0.093	0.093
Scenario 2	0.0954	0.0954	0.0954	0.0954	0.0954	0.0954	0.0954

TABLE 4. The centre frequencies of the second IMFs obtained from the experimental tests.

Sensors No.	1	2	3	4	5	6	7
Undamaged	0.1111	0.1104	0.1149	0.1073	0.114	0.1114	0.1114
Scenario 1	0.0969	0.1005	0.0984	0.1086	0.1073	0.1139	0.1149
Scenario 2	0.1009	0.0858	0.0925	0.0913	0.083	0.1092	0.1132

List of Figures

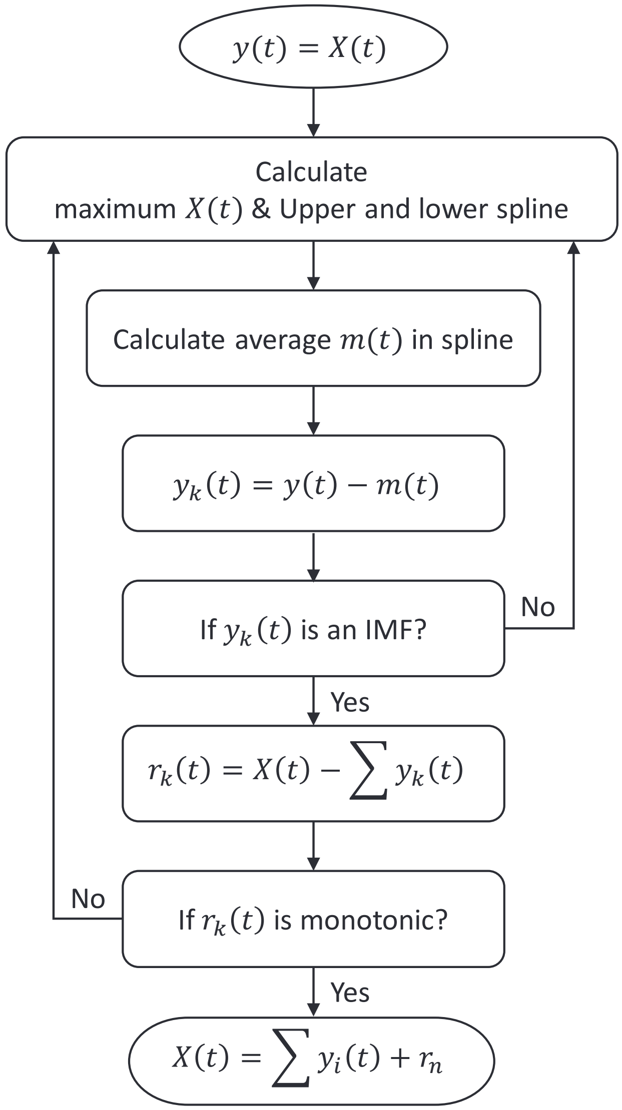

Fig. 1. The flowchart of the EMD algorithm.

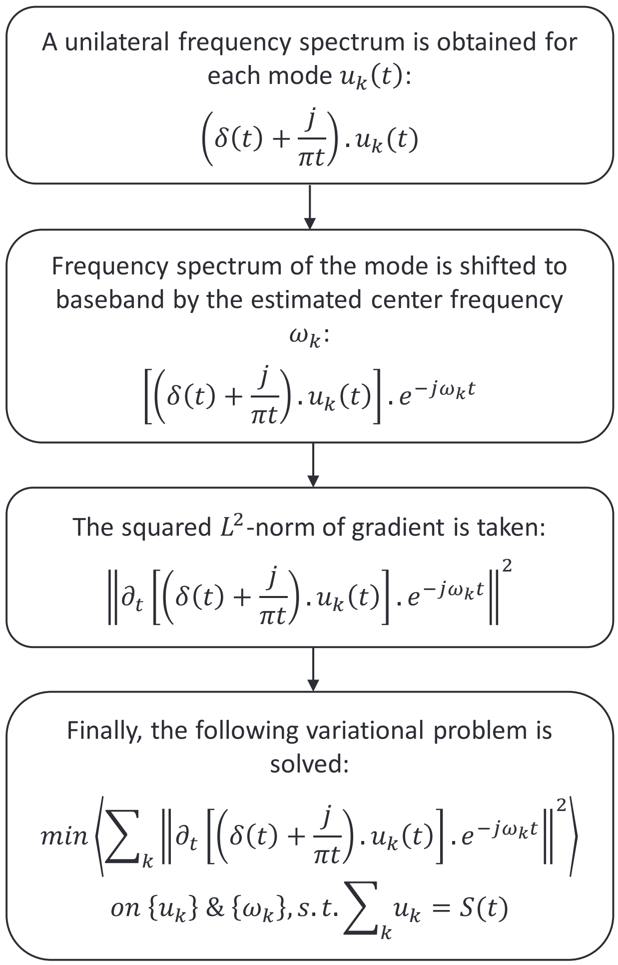

Fig. 2. The VMD algorithm and its steps.

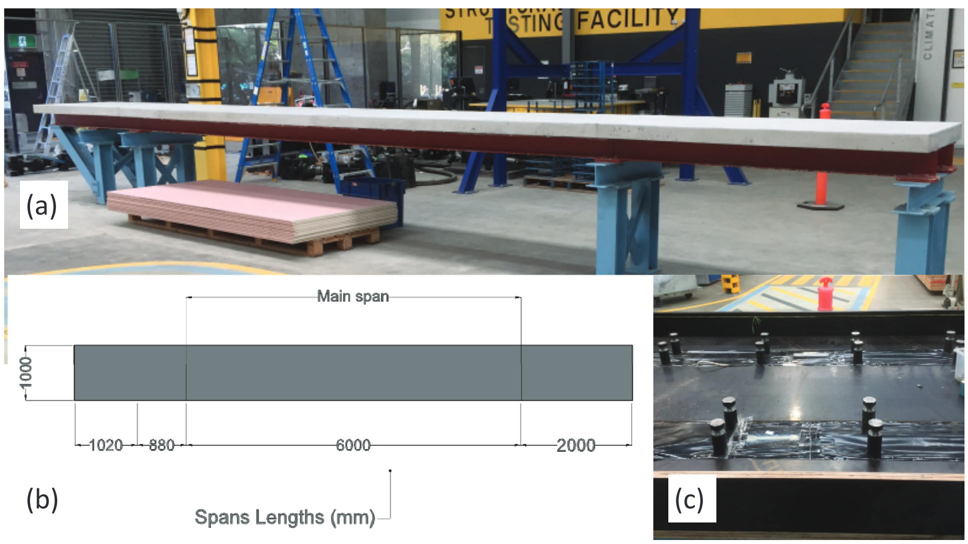

Fig. 3. (a) the bridge model, (b) indicated span and discontinuous slabs end, (c) tube nuts embedded in the concrete slab in the main span for the removable shear connectors (photo taken during construction).

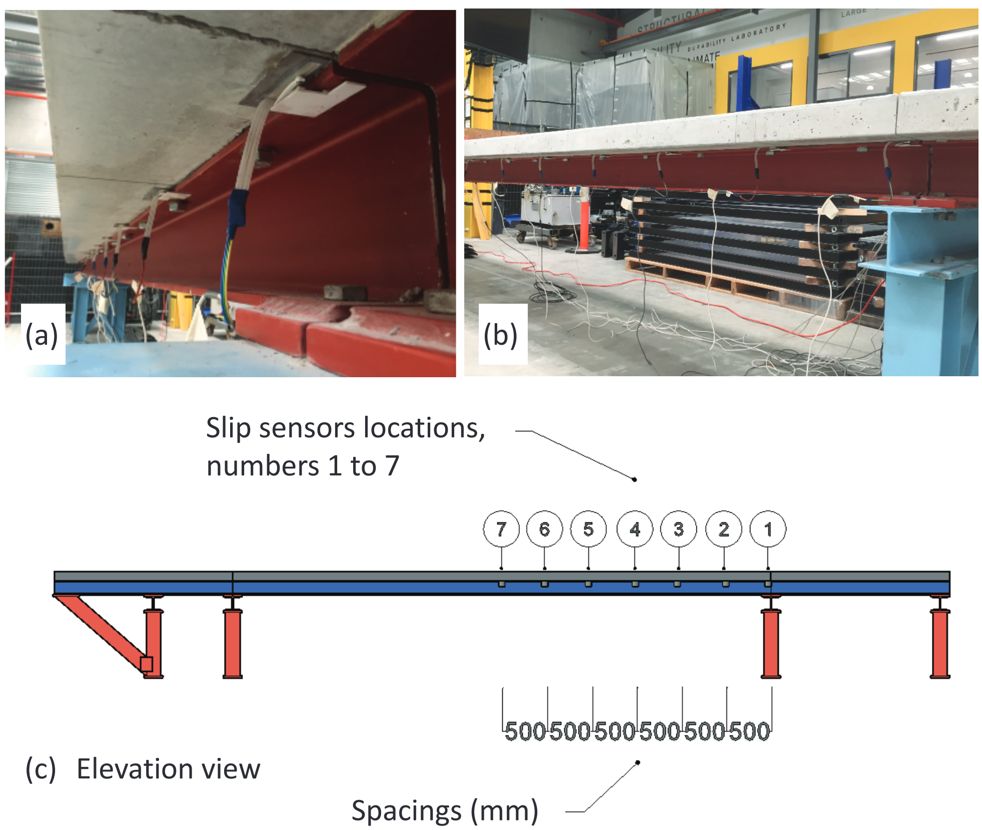

Fig. 4. (a) The installed slip sensors close to support, (b) the slip sensors' locations on the bridge and (c) an elevation sketch of the bridge showing the sensors' numbers and spacings.

Fig. 5. (a) first load case - 375kg, (b) second load case - 750kg, and (c) third load case - 1100kg.

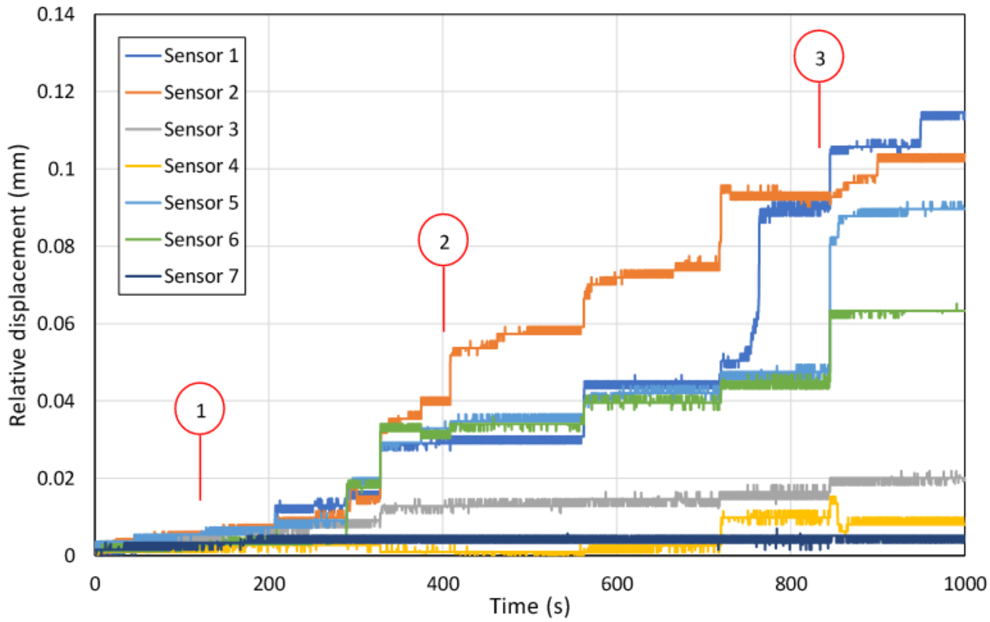

Fig. 6. The relative displacements of the intact bridge under loading.

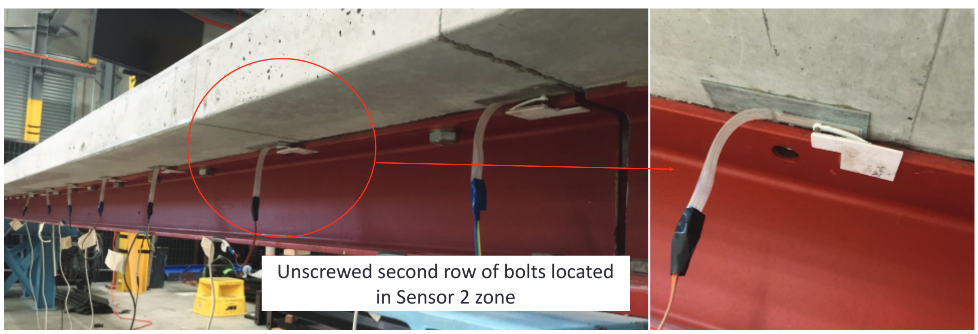

Fig. 7. Second row (both sides of the steel top flange) of bolts which are located in Sensor 2 zone are unscrewed to define single damage.

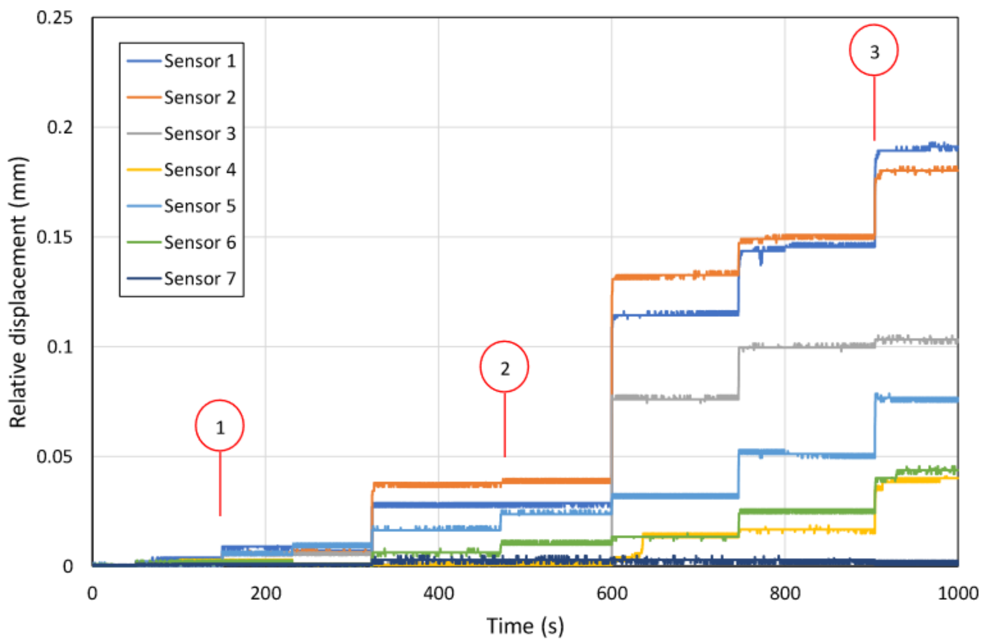

Fig. 8. The relative displacements of the bridge for the single damage scenario.

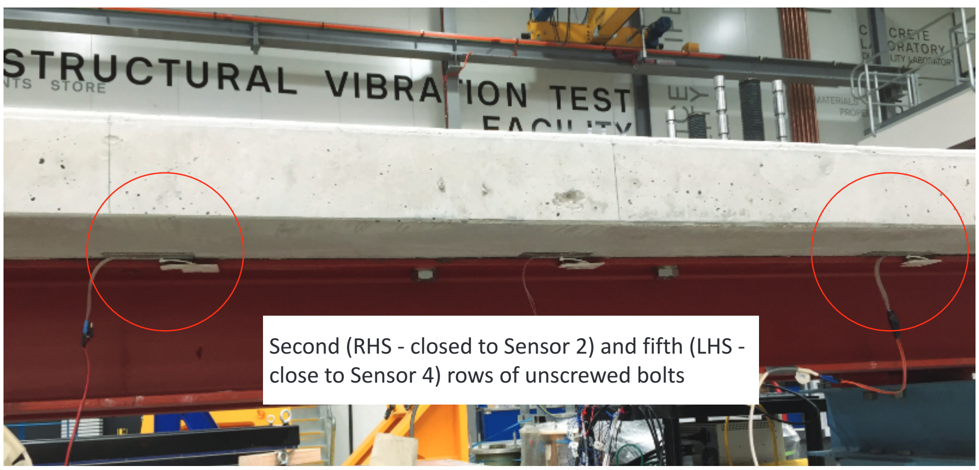

Fig. 9. Second and fifth rows (both sides of the steel top flange) of bolts were unscrewed to define double damage.

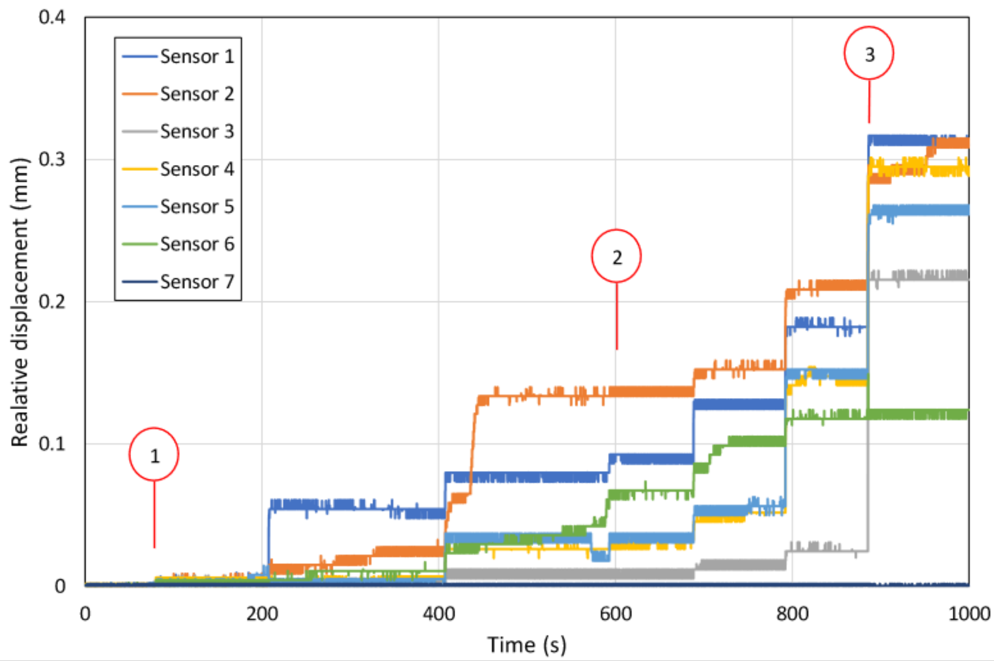

Fig. 10. The shear slip of the bridge for double damage scenario.

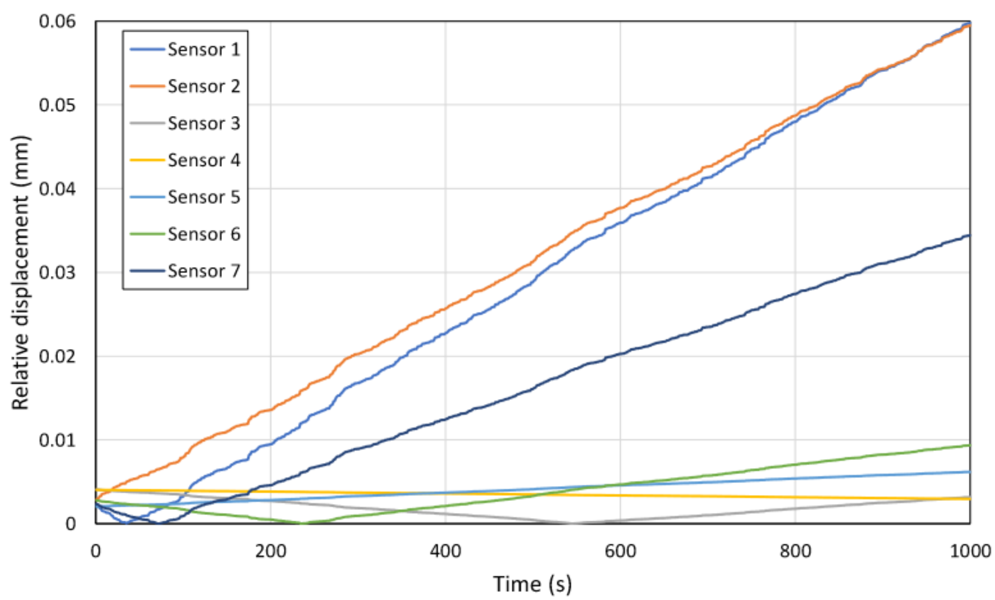

Fig. 11. Relative displacements measured from the FE model of the intact beam in terms of time.

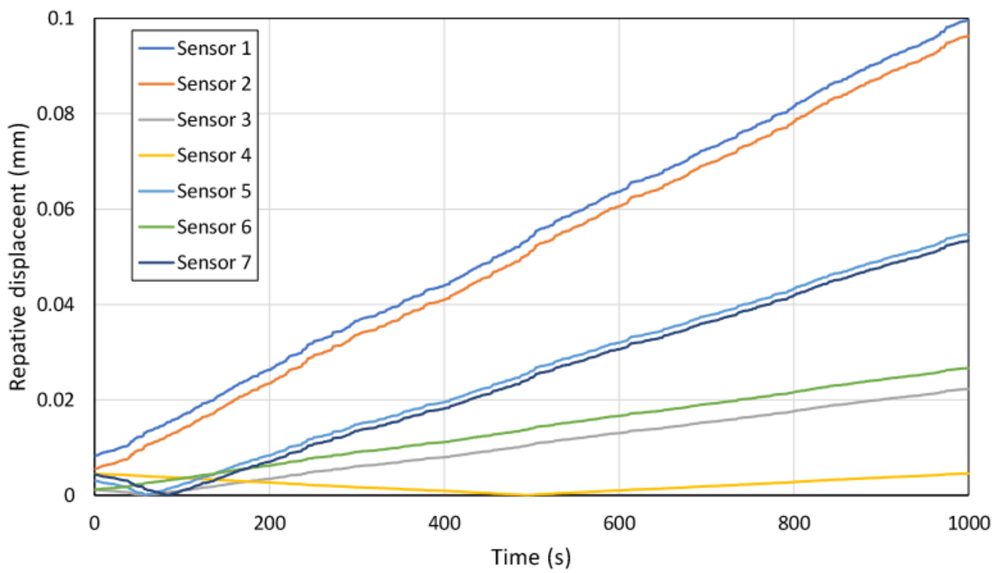

Fig. 12. Relative displacements in terms of time measured from FE model of the beam for damage scenarios 1.

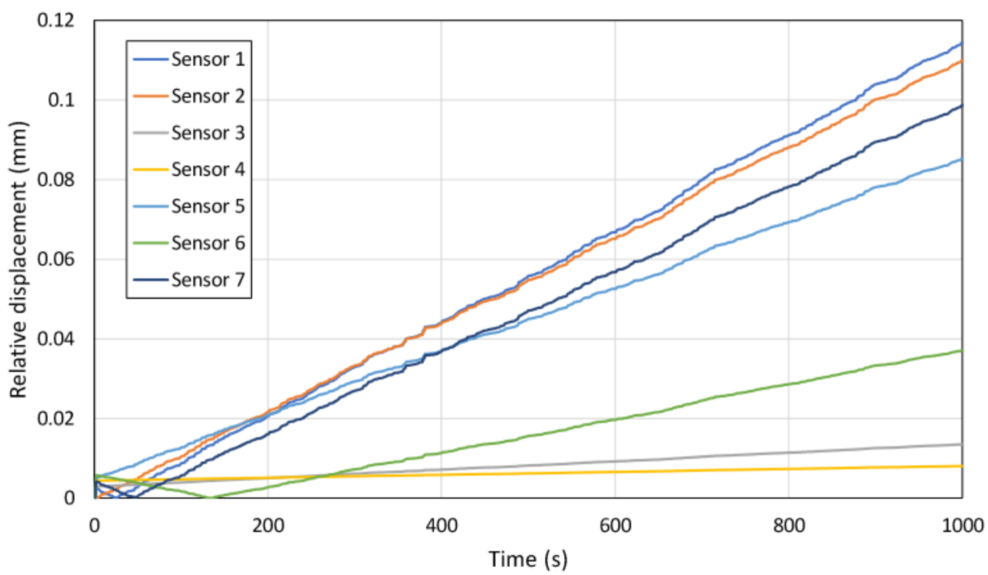

Fig. 13. Relative displacements in terms of time measured from FE model of the beam for damage scenarios 2.

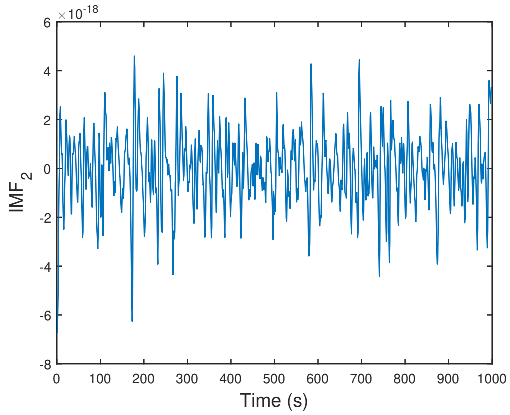

(a) Original IMF2 signal

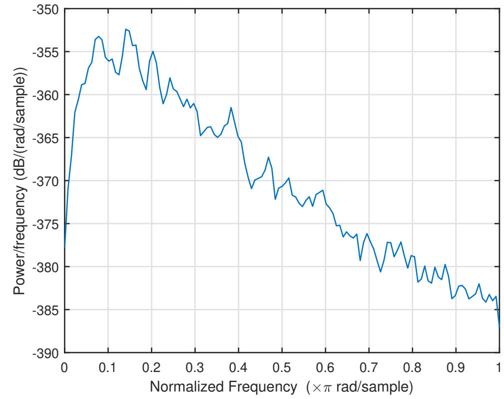

(b) WPSD of IMF2 signal

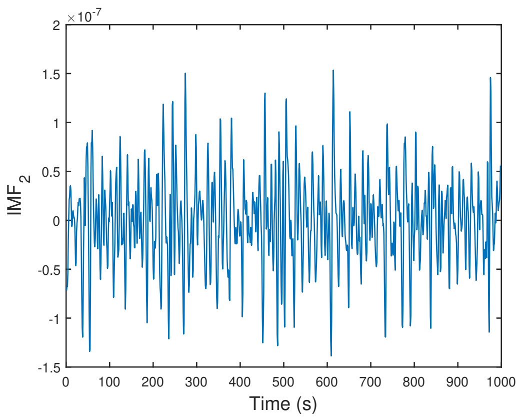

(c) Original IMF2 signal

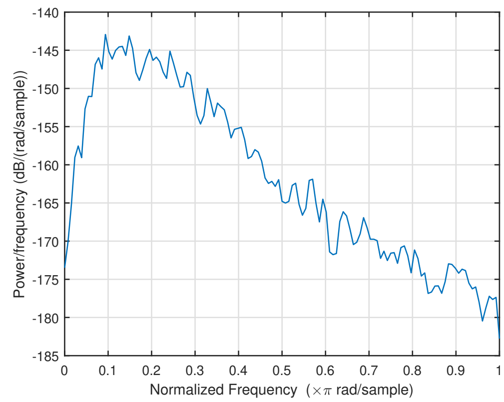

(d) WPSD of IMF2 signal

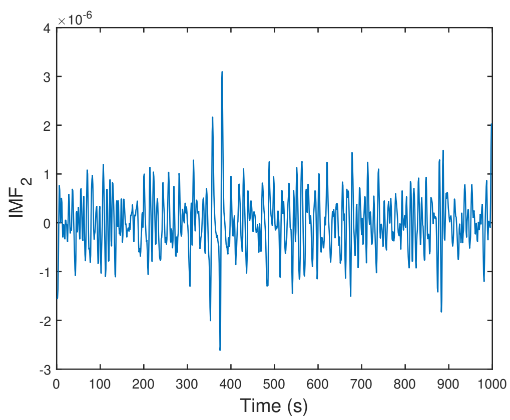

(e) Original IMF2 signal

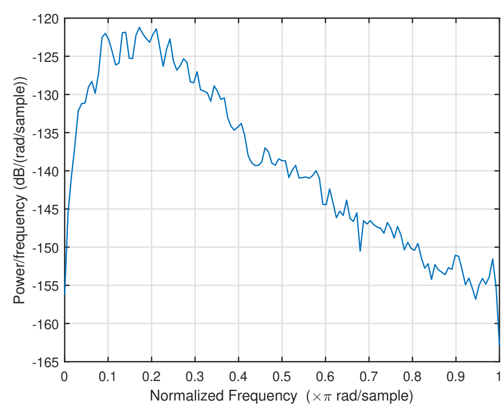

(f) WPSD of IMF2 signal

Fig. 14. The obtained IMF2 signals from the decomposition of the interlayer slip of the FEM model of the beam (LHS plots) and their corresponding WPSD (RHS plots) for different damage scenarios of (a & b) U, (c & d) D1, and (e & f) D2.

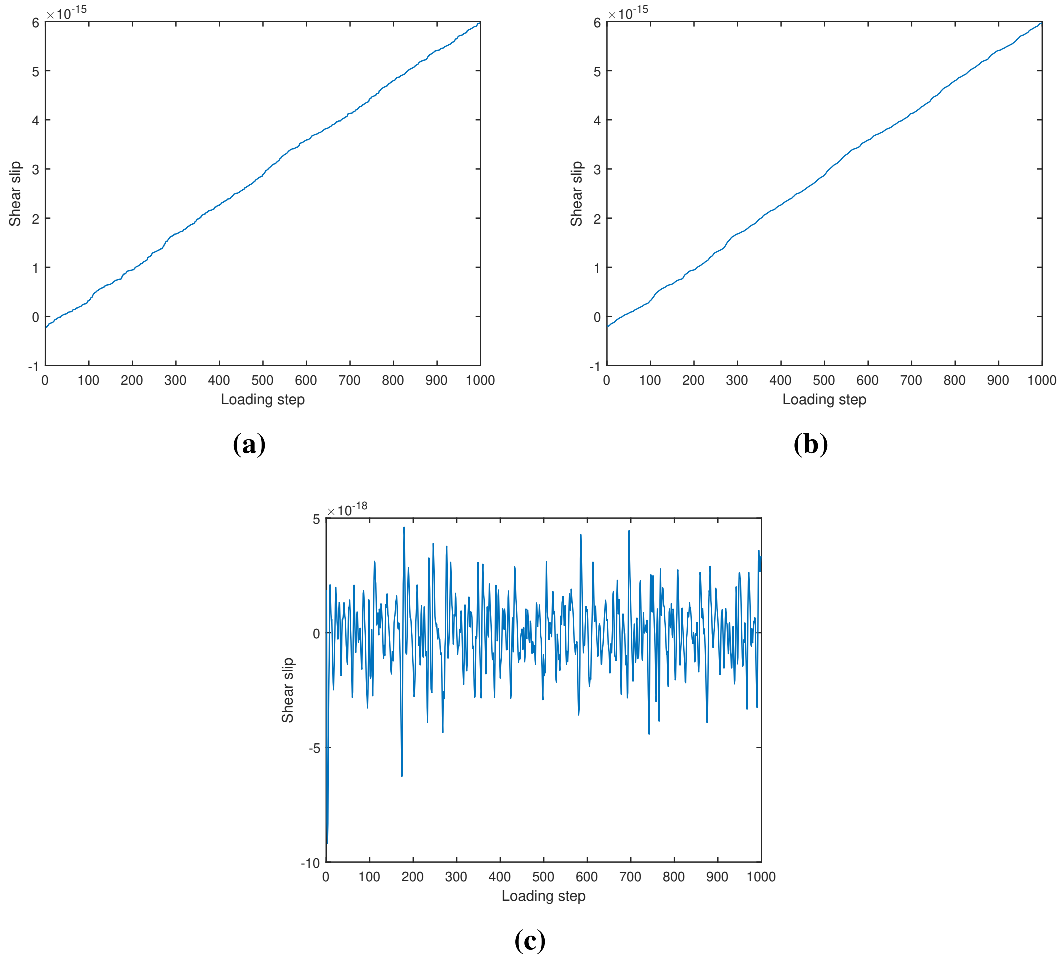

Fig. 15. The shear slip data obtained from the numerical model for the undamaged scenario at Sensor 1; (a) the original signal, (b) IMF 1 and (c) IMF 2 obtained from the VMD.

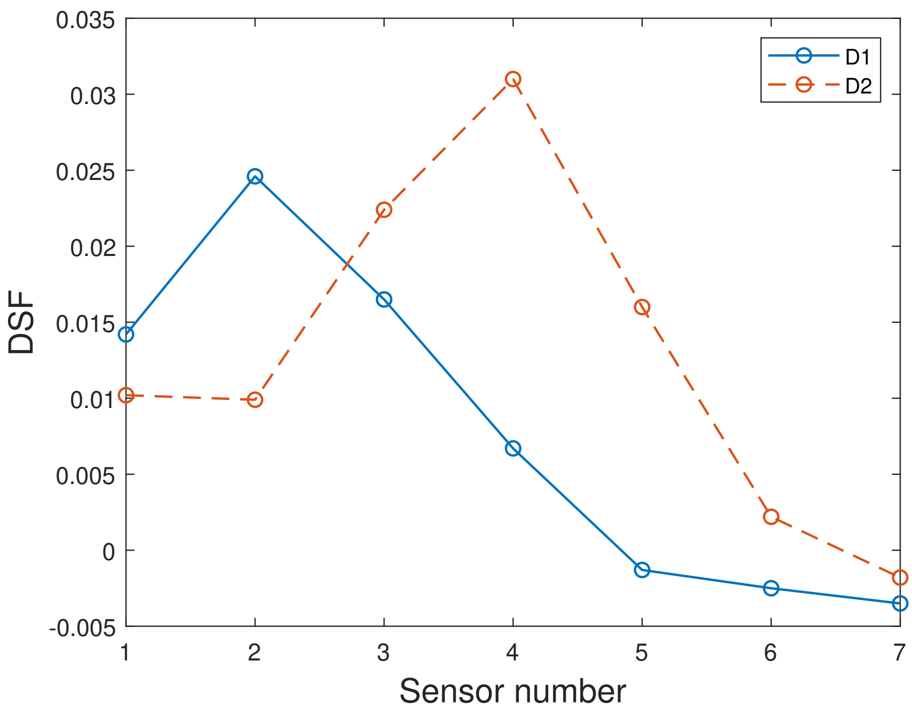

Fig. 16. The value of the DSF obtained for different damage scenarios regarding the experimental study.

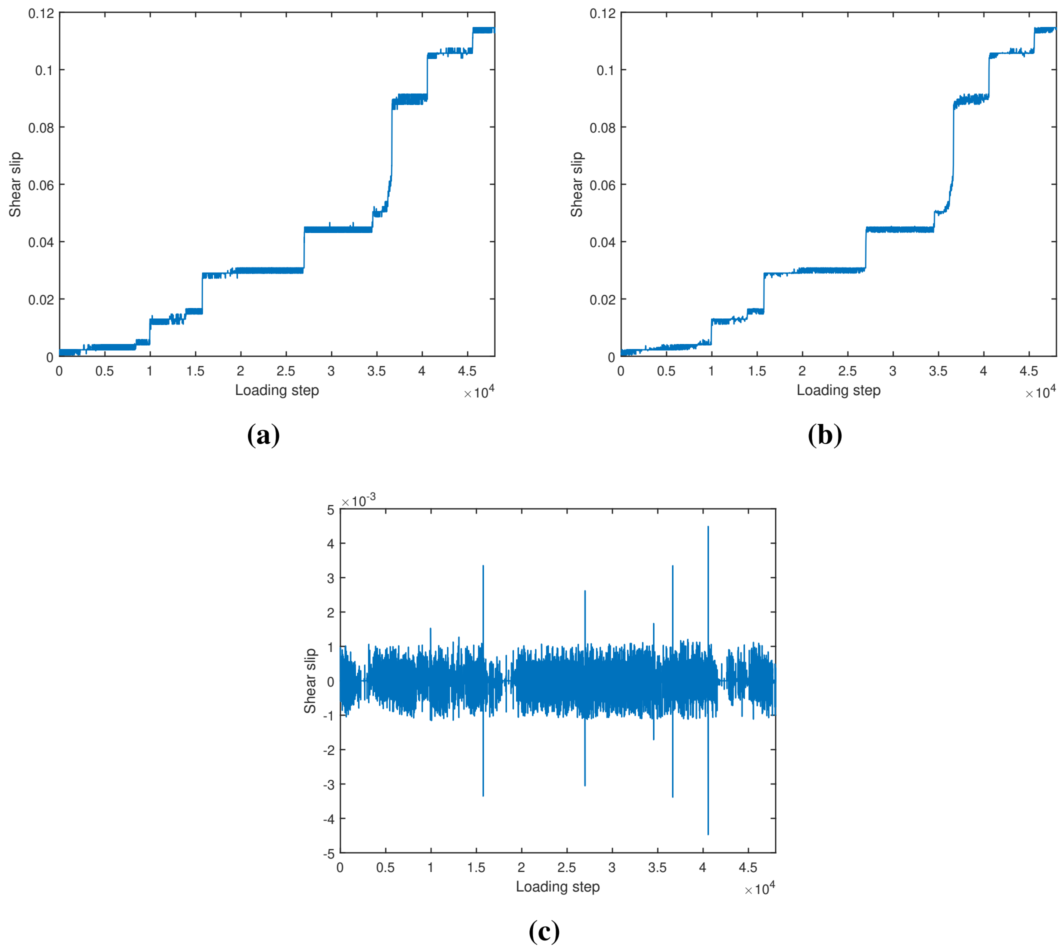

Fig. 17. The shear slip data obtained from the experimental model for undamaged scenario in Sensor 1; (a) the original signal, (b) IMF 1 and (c) IMF 2 obtained from the VMD.

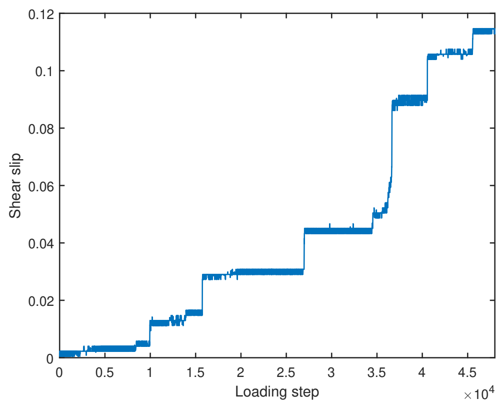

(a)

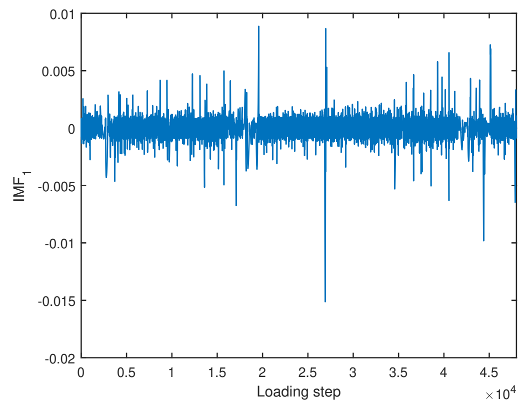

(b)

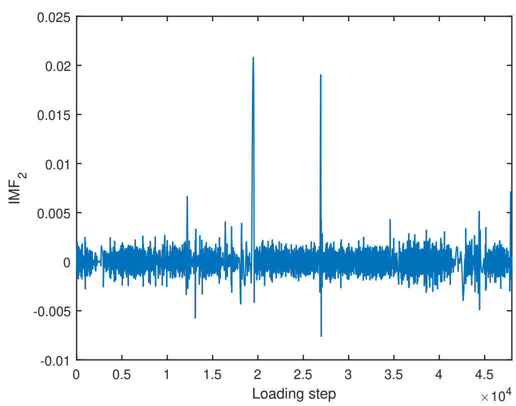

(c)

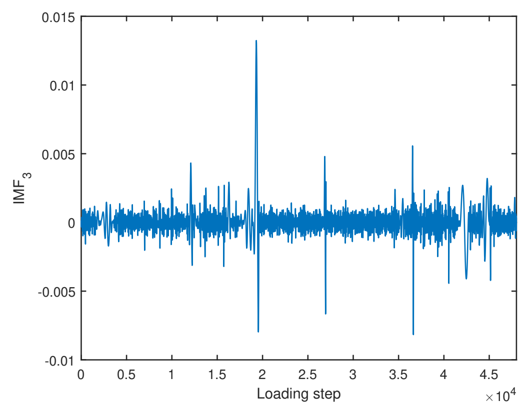

(d)

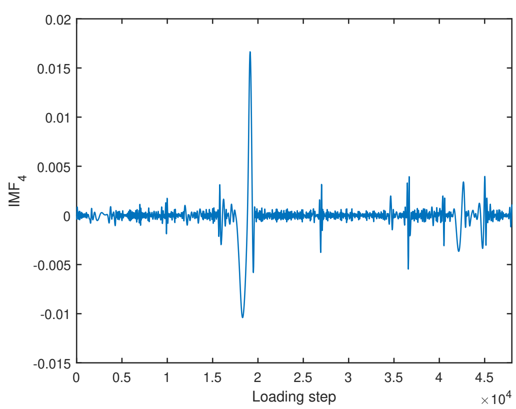

(e)

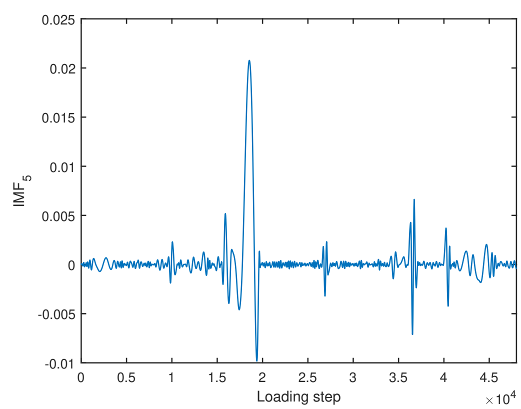

(f)

To be continued on the next page.

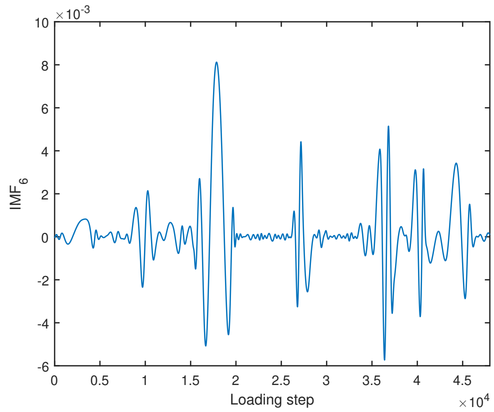

(g)

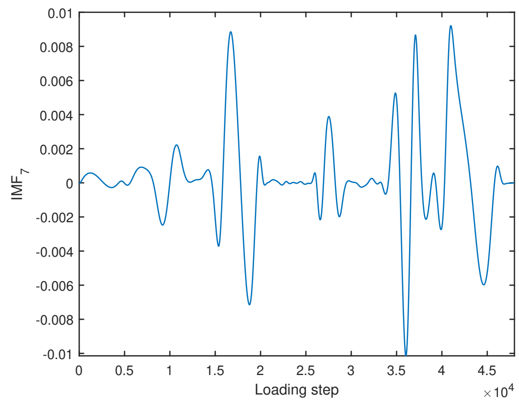

(h)

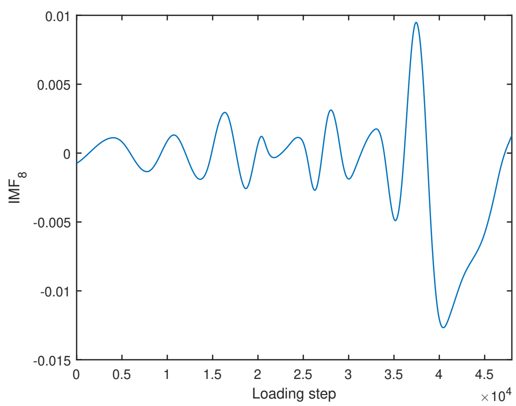

(i)

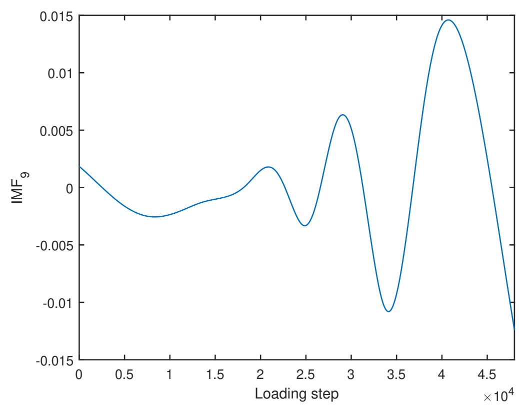

(j)

Fig. 18. Nine IMFs obtained from the decomposition of the shear slip signal using the EMD algorithm; (a) original signal and (b-j) extracted IMFs.

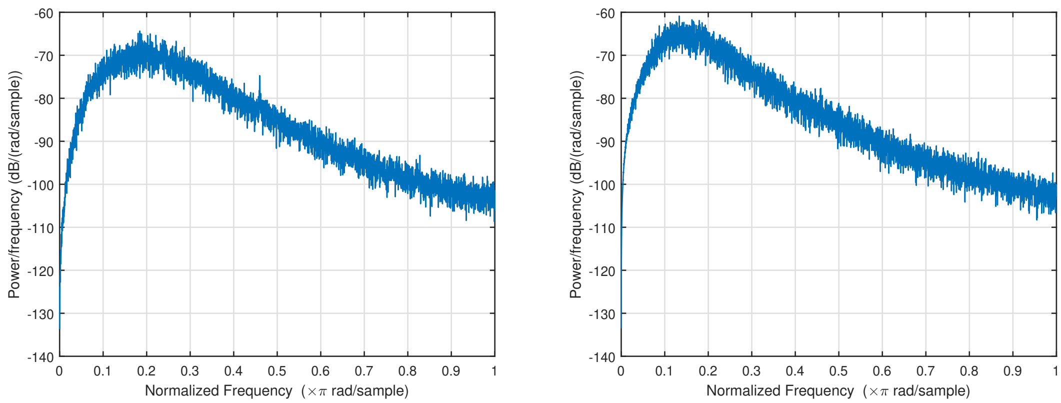

(a) **(b)**

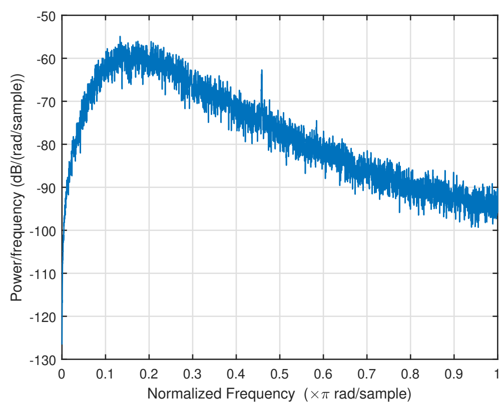

(c)

Fig. 19. WPSD of the signal obtained from sensor 2 mounted on the beam for (a) undamaged, (b) single damage and (c) double damage.